NJC

Accepted Manuscript

This is an *Accepted Manuscript*, which has been through the Royal Society of Chemistry peer review process and has been accepted for publication.

Accepted Manuscripts are published online shortly after acceptance, before technical editing, formatting and proof reading. Using this free service, authors can make their results available to the community, in citable form, before we publish the edited article. We will replace this *Accepted Manuscript* with the edited and formatted *Advance Article* as soon as it is available.

You can find more information about *Accepted Manuscripts* in the Information for Authors.

Please note that technical editing may introduce minor changes to the text and/or graphics, which may alter content. The journal's standard Terms & Conditions and the Ethical guidelines still apply. In no event shall the Royal Society of Chemistry be held responsible for any errors or omissions in this *Accepted Manuscript* or any consequences arising from the use of any information it contains.

ROYAL SOCIETY OF CHEMISTRY

www.rsc.org/njc

Journal Name RSCPublishing

ARTICLE

Photoluminescence and white-light emitting in two series of heteronuclear Pb(II)-Ln(III) complexes

Cite this: DOI: 10.1039/x0xx00000x

Received 00th January 2014,
Accepted 00th January 2014

DOI: 10.1039/x0xx00000x

www.rsc.org/

Cheng Yan[a], Ling Chen[a], Mei Pan[a,b]*, Lu-Yin Zhang[a], Shao-Yun Yin[a], Yi-Xuan Zhu[a], Kai Wu[a], Ya-Jun Hou[a] and Cheng-Yong Su[a]*

Two series of Pb(II)-Ln(III) heteronuclear coordination complexes are assembled from a tripodal ligand triCB-NTB ((4,4',4''-(2,2',2''-nitrilotris(methylene)tris(1*H*-benzo[*d*]imidazole-2,1-diyl)tris(methylene))tribenzoic acid). In **Pb_2LnL_2** series, the Ln^{3+} ion is encapsulated in highly symmetrical {LnO_6} octahedron with an inversion center, and Pb-Ln-Pb clusters are formed by the linkage of carboxyl groups on triCB-NTB ligands to Pb^{2+} and Ln^{3+} simultaneously. While in **$PbLn_2L_2$** series, the Ln^{3+} ion is encapsulated in a distorted {LnO_9} polyhedron without inversion center. Pb^{2+} ions are coordinated with benzimidazole and apical N atoms on the ligand isolatedly, and the carboxyl groups only link two Ln^{3+} ions into Ln-Ln cluster. This structural variation leads to different photoluminescence behaviour in these two series of complexes. Most importantly, the linkage of Pb-Ln-Pb clusters brings more perturbation to the excited states of the ligand. Therefore, more obvious ligand-to-metal charge transfer (LMCT) process is observed in **Pb_2LnL_2** series, and the energy transfer to the accepting levels of Ln^{3+} ions becomes more efficient. Furthermore, the combination of LC (ligand-centered)+LMCT+MC (metal-centered) emissions in complex **Pb_2EuL_2** results in single component white light emission.

Introduction

In solid state lighting field, the development of white light emitting (WLE) devices is one of the hotspots in recent decades, and abundant WLE materials including nanocrystals, polymer and rare earths doped phosphors have been reported by researchers.[1] Generally speaking, the fabrication of white light devices now mainly depends on the combination of multiple units applying either RGB (red, green, blue) three colour or YB (yellow, blue) double colour mixing principle, which inevitably brings such problems as colour impurity, low efficiency, high cost, poor reproducibility, as well as processing difficulty.[2,3] In order to overcome the above drawbacks, the development and utilization of single component white light emitting materials has caused wide attention in recent years.[4,5] Among which, more and more single phase white light emitting supramolecular coordination complexes have been reported since the end of last century, along with the rapid development of supramolecular materials and supramolecular chemistry.[6-8] In contrast, the reports of heteronuclear coordination complexes based on IV/VA main group (such as bismuth, tin, lead, antimony, etc.) and lanthanide elements still remains rare, even less are explored for their single phase white light emitting properties.[9,10] In fact, the Pb and Bi elements have unique lone pair electron effects (with ns^2np^0 configuration) and flexible coordination contributes, which affords them with special superiority in structural regulation and light emitting modulation.[11] Especially, the LMCT (ligand to metal charge transfer) or MC (metal-centered) transitions involving the *s* and *p* orbitals of Pb(II) ions may endow wide-band emission in Pb(II)-containing complexes,[12,13] and the combination with characteristic emissions from Ln(III) ions further provides versatile luminescent properties and white-light emitting possibilities in Pb(II)-Ln(III) heteronuclear complexes.

We report herein two series of Pb(II)-Ln(III) heteronuclear coordination complexes based on one NTB-substituted tripodal ligand (triCB-NTB, H_3L). [14] By the alteration of Pb:Ln metal ratio, different coordination structures and luminescent properties are obtained. Especially, unique Pb-Ln-Pb clusters are formed in the structure of **Pb_2LnL_2** series, and the combination of LMCT-related with lanthanide-centered emissions in complex **Pb_2EuL_2** leads to single-component white light photoluminescence tunable by excitation wavelength.

Results and discussion

Crystal structures

Initial exploration of the unit cells by preparatory single-crystal X-ray analyses of complexes **Pb_2LnL_2** series proves that

the four complexes are isostructural, which are further confirmed by powder X-ray diffraction as shown in Fig. S1. Therefore, we only take complex **Pb_2TbL_2** as a representative to show the crystal structure. Complex **Pb_2TbL_2** crystallizes in the monoclinic $P2_1/n$ space group and the asymmetric unit contains one Pb^{2+}, a half Tb^{3+}, one L^{3-} ligand, a half uncoordinated NO_3^- anion, one solvated DMF and water molecules. The Pb^{2+} ion lies in a seven-coordinated geometry, surrounded by four N atoms from one L^{3-} ligand, and three carboxyl O atoms from three other L^{3-} ligands, forming a $\{PbO_3N_4\}$ distorted face-capped trigonal prismatic coordination environment. The Pb−N distances are ranged from 2.49 to 2.82 Å, and Pb−O distances from 2.51 to 2.80 Å. Meanwhile, each Tb^{3+} ion is entrapped in a $\{TbO_6\}$ octahedron by six benzoic arms from four L^{3-} ligands (Fig. 1a). The $\{TbO_6\}$ octahedral are quite regular, with Tb−O distances between 2.24 to 2.28 Å, and O−Tb−O angles from 89.2 to 92.2°, showing the high coordination symmetry with an inversion center around Tb^{3+} metal ions (Fig. 1b). It is noted that all the carboxyl groups on benzoic arms of the ligands coordinate with one Pb^{2+} and one Tb^{3+} simultaneously in a μ-fashion, forming Pb-Tb-Pb clusters linked by L^{3-} ligands into a three dimensional network (Fig. 1c). From the structure, we can isolate a loop-and-chain structure by the linkage of box-like loops enclosed by two Pb^{2+} ions and two Pb-Tb-Pb clusters (Figs. 1d and S3). To our knowledge, this is the first example of such kinds of cluster formed between Pb(II) and Ln(III) linked by carboxyl groups.

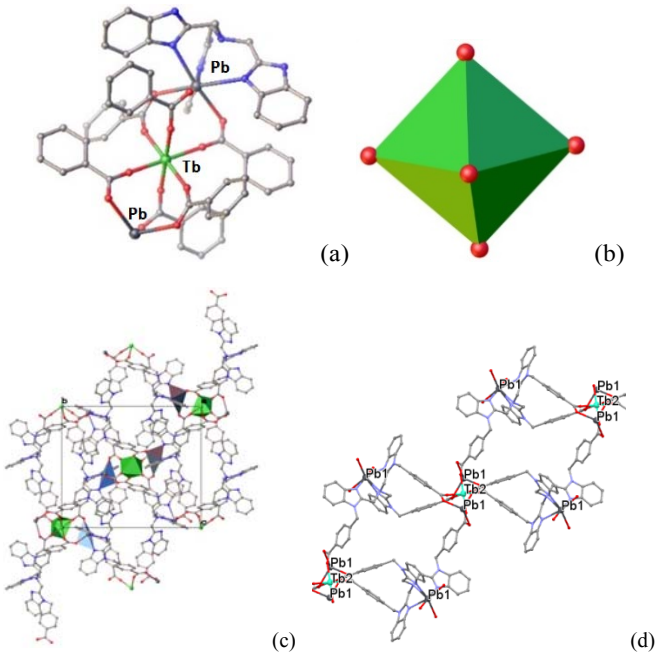

Fig. 1 Structure of complex **Pb_2TbL_2**: (a) Pb-Tb-Pb cluster; (b) $\{TbO_6\}$ coordination polyhedron; (c) crystal packing along *a* direction showing coordination polyhedra around Pb^{2+} and Tb^{3+}; (d) linkage of molecular "box" (Tb green, Pb purple gray, N blue, C gray, O red, H atoms, uncoordinated anions and solvated molecules are omitted for clarity).

Complexes **$PbLn_2L_2$** series are also isostructural as proved by powder X-ray diffraction (Fig. S2). And we take complex **$PbTb_2L_2$** as a representative, which crystallizes in the triclinic $P\bar{1}$ space group and the asymmetric unit contains one Tb^{3+}, a half Pb^{2+}, one L^{3-} ligand, one coordinated NO_3^- anion, one uncoordinated DMF and three water molecules. Different from the above series, each Tb^{3+} is coordinated with seven carboxyl O atoms from four L^{3-} ligands, together with two O atoms from one NO_3^- anion, forming a $\{TbO_9\}$ distorted polyhedron without inversion center. The Tb−O distances are ranged from 2.49 to 2.82 Å. The carboxyl groups from different ligands link two Tb^{3+} ions into a paddle-wheel shaped Tb-Tb cluster, with a Tb-Tb distance of 3.95 Å (Figs. 2a and 2b). In comparison, the Pb^{2+} ions are coordinated with six N atoms from two L^{3-} ligands, forming nearly cubic geometry. The Pb−N distances in $\{PbN_6\}$ polyhedron are all within 2.66 to 2.71 Å, presenting a higher coordination symmetry environment around Pb^{2+} compared with that in the first series (Fig. 2c). From the view of one triCB-NTB ligand, two of its three substituted para-methyl carboxylic benzene arms extend in the same direction, coordinated with a Tb^{3+} center in a bidentate μ-fashion. The third carboxylic benzene is positioned in a nearly perpendicular way relative to the former two, and is simultaneously coordinated with two Tb^{3+}. Therefore, two triCB-NTB ligands link two Pb^{2+} ions and two Tb-Tb clusters together into a box-like loop. It is further extended in 1D direction to form a loop-and-chain structure, which looks similar to that in the **Pb_2LnL_2** series, while the linking metallic nodes are different (Figs. 2d and S4). The chains are further packed together in the crystal lattice due to the π–π interactions between the aromatic rings (distance 3.53 Å) and the hydrogen bonds formed between the oxygen atoms of guest water molecules and coordinated water molecules or carboxylate groups on the ligands (distance 2.69 to 2.99 Å).

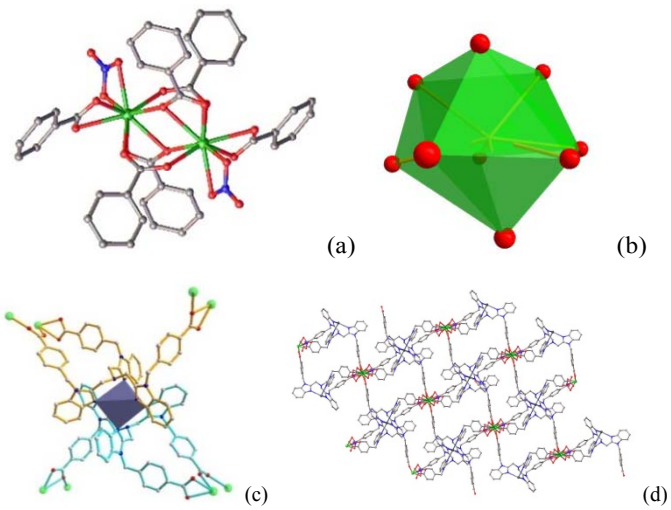

Fig. 2 Structure of complex **$PbTb_2L_2$**: (a) coordination geometry of Tb-Tb cluster; (b) $\{TbO_9\}$ coordination polyhedron; (c) coordination geometry of Pb^{2+} (represented by purple gray polyhedron) and neighboring Eu^{3+} ions; (d) linkage of molecular "box" (Tb green, Pb purple gray, N blue, C gray, O red, H atoms and solvated molecules are omitted for clarity).

Photoluminescence properties

In order to analyze the luminescent behaviour of the above two series of Pb(II)-Ln(III) complexes, we first probe the emissions of complexes **Pb_2GdL_2** and **$PbGd_2L_2$**. Since the lowest excited state of Gd^{3+} ions is higher than 31,000 cm^{-1}, well above the excited state of the ligand, the energy transfer from the ligand to Gd^{3+} ions will be blocked. Therefore, the detection of ligand-based luminescence will be more unambiguous. From the emission spectra of **Pb_2GdL_2** and **$PbGd_2L_2$** excited at 370 nm (Fig. 3), we can see that the emission of complex **Pb_2GdL_2** is obviously red-shifted compared with the latter. At the same time, the emission contour of **Pb_2GdL_2** is also more structured, in which three broad peaks at 440, 470 and 530 nm are observed. Among which, the highest energy band at 440 nm can be assigned to the ligand-centered (LC) emission (in accordance with the emission spectra of triCB-NTB ligand as shown in Fig. S5), and the two lower energy bands at 470 and 550 nm should be related with ligand to metal charge transfer (LMCT) states in the complex. In comparison, only one broad band with a maximum at 440 nm can be observed in complex **$PbGd_2L_2$**, which is dominated by LC emission, and the longer-wavelength emissions related with LMCT states decay rapidly. This difference is closely associated with the different coordination structure in the two series of complexes. In **$PbGd_2L_2$**, the Pb^{2+} ion is coordinated with the benzimidazole and apical N atoms on the ligand and has little effects on perturbing its spectroscopic properties. While in **Pb_2GdL_2**, the triCB-NTB ligand simultaneously links Pb^{2+} and Gd^{3+} through the carboxyl groups, forming $\{Pb_2GdO_x\}$ cluster and leading to strong energy coupling interchanges among the three counterparts of Pb^{2+}, Gd^{3+} and the ligand. Therefore, the LMCT process in **Pb_2GdL_2** complex is more effective and results in red-shift of the emitting band. The luminescent decay lifetime detected at 470 nm (λ_{ex}=405 nm, laser) for complex **Pb_2GdL_2** is about 1.4 ns and that for **$PbGd_2L_2$** at 440 nm (λ_{ex}=405 nm, laser) is about 1.2 ns, both relating to the short domain lifetime. This excludes the possibility of phosphorescence from the $^3\pi\pi^*$ triplet states of the ligand and confirm the assignment of either LMCT or LC-based singlet state photoluminescence.

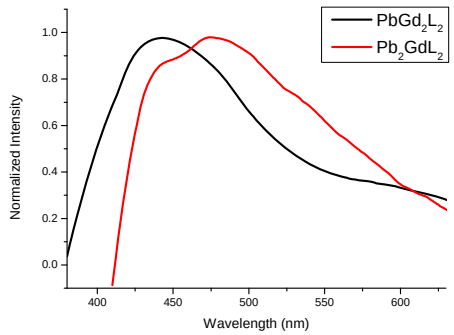

Fig. 3 Emission spectra of complexes **Pb_2GdL_2** and **$PbGd_2L_2$** excited at 370 nm in solid state.

To further study the energy transfer from the triCB-NTB ligand to lanthanide ions with suitable accepting energy levels, emission spectra were tested for the above two series of Pb(II)-Ln(III) complexes and shown in Figs. 4-6. As we can see, upon the addition of emitting lanthanide ions, the ligand based emission from 400 to 550 nm is greatly attenuated. Meanwhile, the characteristic lanthanide emissions appear at corresponding wavelengths, showing obvious energy transfer from the ligand to Ln(III) ions.

Specifically, for complex **Pb_2EuL_2**, there are basically two groups of emission bands, i.e., the broad band covering 400 to 550 nm correlated with the Pb^{2+}-involved LC and LMCT emissions, and the characteristic sharp peaks from the $^5D_0 \rightarrow {}^7F_J$ f-f transitions of Eu^{3+} ions (Fig. 4a). Furthermore, the relative intensities between the two groups of emission bands can be adjusted by different excitation wavelength. At the excitation of higher energy wavelength from 290 to 330 nm, the ligand-involved emissions are very weak, and the Eu^{3+}-centered emissions dominate. Therefore, the photoluminescence of complex **Pb_2EuL_2** is basically in the red-light area as calculated by CIE coordinates (Fig. 4b). At the excitation of 350 to 370 nm, the combination of LC+LMCT emissions and Eu^{3+}-centered emissions results in light emitting of orange colour. And at the excitation of 380 to 400 nm, the intensities of the two groups of emission bands become comparable, therefore white light emitting is produced. For the emissions excited at 380, 390 and 400 nm, the calculated CIE coordinates are at (0.412, 0.333), (0.404, 0.317), and (0.345, 0.343), all falling into the white light zone (Fig. 4b). The above variations in the photoluminescence spectra of complex **Pb_2EuL_2** manifests that energy transfer from the sensitizer (ligand) to acceptor (lanthanide) can be more complete with higher energy excitation before 330 nm, while incomplete energy transfer between the two parts with lower energy excitation after 380 nm leads to white light combination. The excitation spectra (Fig. S6) detected at ligand based emission (450 nm) and lanthanide based emission (617 nm) fully support the above changes in energy transfer tendency. As a candidate application in WLE devices, the thermal stability of complex **Pb_2EuL_2** is tested and shown in Fig. S8. As we can see, the complex can be stable up to 280 °C and then begins to collapse, which is acceptable as a coordination compound, although not good enough compared with pure inorganic phosphors.[1,15]

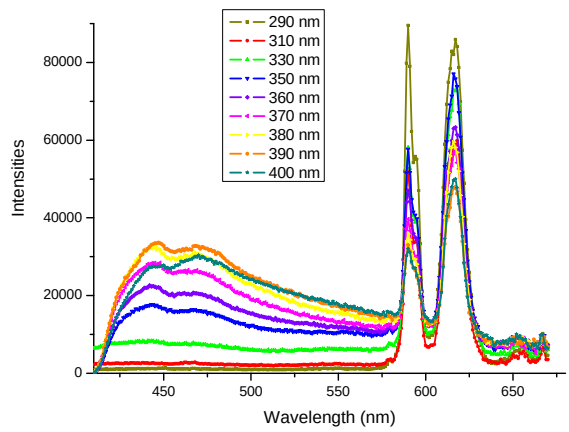

a)

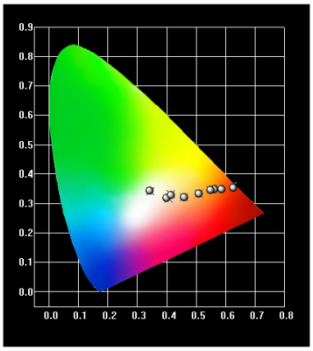

b)

Fig. 4 (a) Emission spectra by excitation wavelength from 290 to 400 nm, and (b) CIE coordinates at the excitation from 290 to 400 nm (showing in dot symbols from right to left, referring to the excitation wavelength at 290, 310, 330, 350, 360, 370, 380, 390 and 400 nm, respectively) for complex **Pb_2EuL_2** at room temperature.

In comparison, the photoluminescence of **$PbEu_2L_2$** shows less contribution from the ligand-involved emission (Fig. 5a). Similar to complex **Pb_2EuL_2**, by the excitation wavelength at higher energy band from 290 to 330 nm, only Eu^{3+}-based emission can be detected. While by the longer wavelength excitation from 350 to 400 nm, the LC-based emission appears in complex **$PbEu_2L_2$**, but the intensity is rather weak. As a consequence, the combined photoluminescence from the two parts of ligand and Eu^{3+} does not enter the white-light emitting area (Fig. 5a inset). Furthermore, we can also detect a clear difference in the Eu^{3+}-emitting photoluminescence. As a representative, the emission spectra of complexes **Pb_2EuL_2** and **$PbEu_2L_2$** excited at 290 nm are shown in Fig. 5b. We can see that for **Pb_2EuL_2** , the intensities for the two emitting peaks at 590 and 612 nm are almost identical, while for **$PbEu_2L_2$**, the relative intensity of I_2 (612 nm)/I_1 (590 nm) is more than 10-fold. This difference can also be found by the direct excitation of Eu^{3+} absorption at 395 nm (Fig. S9) and manifests the distinct structural character in these two complexes. For Eu^{3+}, the $^5D_0 \rightarrow {}^7F_1$ transition at about 590 nm is a magnetic dipole allowed transition (MD), while the $^5D_0 \rightarrow {}^7F_2$ at 612 nm is belonging to an electric induced dipole transition (ED). In general, when the Eu^{3+} ion is located in a lower-symmetry coordination environment without inversion center, the $^5D_0 \rightarrow {}^7F_2$ transition is predominant, and in a highly symmetrical coordination environment, the $^5D_0 \rightarrow {}^7F_1$ transition becomes stronger. That is just the case observed in complexes **Pb_2EuL_2** and **$PbEu_2L_2$**, in which the former forms a $\{LnO_6\}$ octahedron with high symmetry, while in the latter, a $\{LnO_9\}$ distorted polyhedron without inversion center can be found.[16] Comparison between the luminescent lifetime (1.38 ms for **Pb_2EuL_2** and 0.42 ms for **$PbEu_2L_2$**, λ_{em}= 612 nm, λ_{ex}=290 nm) and quantum efficiency (17.8% for **Pb_2EuL_2** and 6.7% for **$PbEu_2L_2$**, λ_{ex}=290 nm) in the two complexes proves that, the Pb^{2+} involvement can perturb the excited states of the ligand and promote more efficient energy transfer to the accepting levels of Eu^{3+} ions.

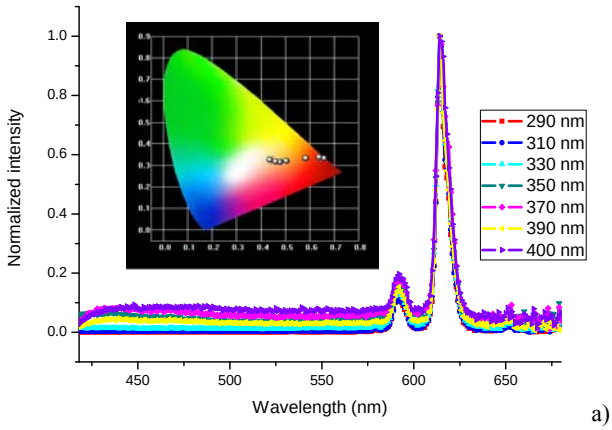

a)

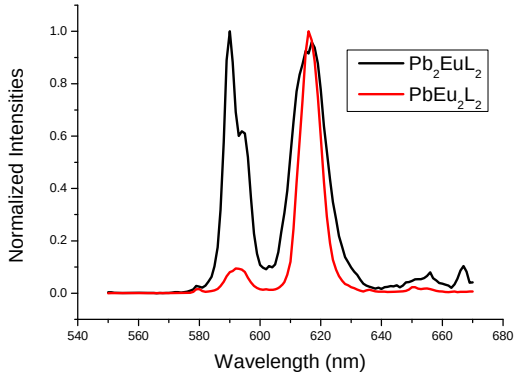

b)

Fig. 5 (a) Emission spectra at the excitation wavelength from 290 to 400 nm for complex **PbEu$_2$L2** at room temperature (the inset shows the calculated CIE coordinates by dot symbols, referring to the excitation wavelength at 290, 310, 330, 350, 370, 390 and 400 nm from right to left, respectively), and (b) comparison between the emission spectra of complexes **Pb$_2$EuL2 and PbEu$_2$L2** at the excitation of 290 nm.

Similarly, we can also detect a clear difference in the photoluminescence spectra of complexes **Pb_2SmL2** and **$PbSm_2L2$** (Fig. 6a). For Sm^{3+}, the $^4G_{5/2} \rightarrow {}^6H_{7/2}$ transition at 600 nm is magnetic dipole allowed (MD), while the $^4G_{5/2} \rightarrow {}^6H_{9/2}$ transition at 650 nm is electric dipole allowed (ED),[15c] which will become predominant in an unsymmetrical coordination environment. This tendency can be manifested by the relative intensity ratio of I_2 (650 nm)/I_1 (600 nm) in the two complexes, which is ~0.5 for **Pb_2SmL_2** and ~2.0 for **$PbSm_2L_2$**, respectively, in accordance with their different coordination symmetry. Meanwhile, although the emission contour of complexes **Pb_2TbL_2** and **$PbTb_2L_2$** does not show much difference (Fig. 6b), the luminescent decay lifetimes for the two complexes are quite different. The decay lifetime detected for **Pb_2TbL_2** is about 1.38 ms, almost double that for **$PbTb_2L_2$** (0.77 ms, λ_{em}= 545 nm, λ_{ex}=290 nm). Quantum efficiency test also proves the more efficient energy transfer in complex **Pb_2TbL_2** (35.8%) than in **$PbTb_2L_2$** (23.5%, λ_{ex}=290 nm).

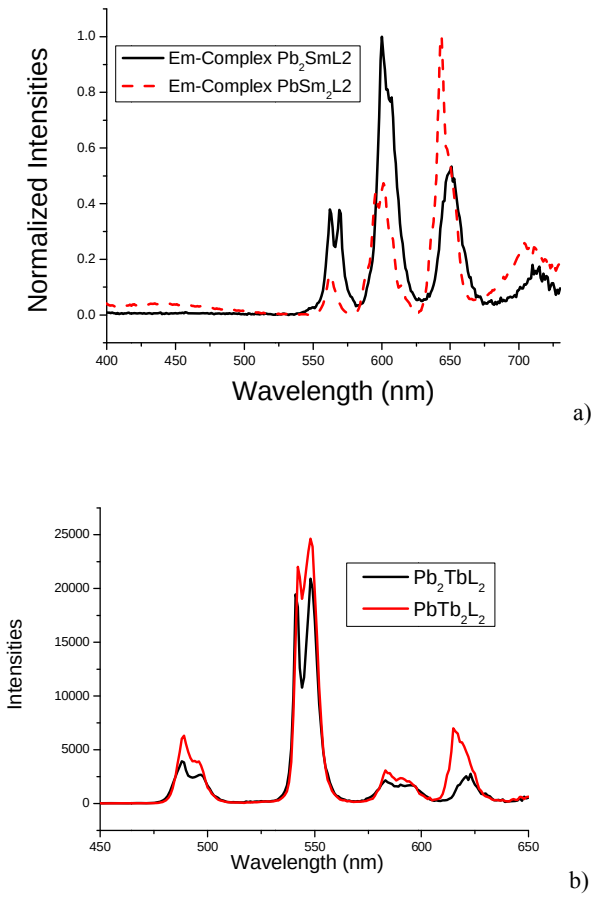

Fig. 6 Emission spectra of complexes **Pb_2SmL_2/$PbSm_2L_2$** (a), and **Pb_2TbL_2/$PbTb_2L_2$** (b) excited at 290 nm in the solid state.

Conclusions

In summary, Pb^{2+} and Ln^{3+} ions are co-assembled into two series of d-f heteronuclear coordination polymers. By varying the ratio between Pb^{2+} and Ln^{3+} species, the coordination polyhedra around the metal centers are greatly altered. Among which, {LnO_6} octahedron with high symmetry and Pb−Ln−Pb cluster by the linkage of carboxyl groups on the ligand are formed in **Pb_2LnL_2** series of complexes. This results in specific emitting contour in some lanthanide complexes (especially for Eu^{3+} and Sm^{3+}), and most importantly, strong perturbation with the excited states of the ligand by Pb^{2+} leads to intensified LMCT (ligand-to-metal charge transfer) process. Therefore, obvious red-shift of the emitting bands from the ligand part can be found. Furthermore, the perturbation of Pb^{2+} ions also promote efficient energy transfer from the ligand to the accepting levels of Ln^{3+} ions, and the combination of LC(ligand-centered)+LMCT+MC(metal-centered) emissions provides single component white light emission in complex **Pb_2EuL_2**. On the other hand, the series of **$PbLn_2L_2$** complexes possess different coordination characters and the corresponding luminescent properties are also different, in which weak LMCT process is observed. This is the first detailed study of the combinational photoluminescence from Pb(II)-Ln(III) heteronuclear complexes with different metallic linking clusters, which will shed some light on the further design and synthesis of more efficient photoluminescent materials involving both lanthanide and main group metals.

Experimental

Materials and methods

All raw materials and solvents were obtained from commercial sources and used without further purification. ^{1}H NMR spectra were measured on a Varian/Mercury-Plus 300 instrument. The C, H, and N elemental analyses were performed on a Perkin-Elmer 240 elemental analyzer. IR spectra were measured on a Nicolet/Nexus-670 FT-IR spectrometer with KBr pellets in the range 4000–400 cm^{-1}. Powder X-ray diffraction (PXRD) data were recorded on a Bruker D8 ADVANCE X-ray powder diffractometer (Cu-Kα, λ = 1.5418 Å). Photoluminescence spectra were taken at room temperature on an EDINBURGH FLS920 fluorescence spectrophotometer. Emission and excitation spectra were corrected for source intensity (lamp and grating) by standard correction curves. A pulsed xenon lamp was used to excite the sample. Decay lifetime tests were performed using the multichannel scaling (MCS) and single-photon-counting options. EPL405 laser (100 *ps*~50 *μs*) or *μ*F900 flashlamp (400 *ns*~10 *s*) excitation was used for lifetime tests in *ns* or *ms* scale, respectively. The excitation sources were mounted directly on the sample chamber at 90° to a double-grating emission monochromator and collected using a single-photon-counting detector. The photons collected at the detector were correlated using a time-to-amplitude converter to the excitation pulse. And the decay lifetime data fitting was based on exponential equation, $I_t = I_1e^{-t/\tau 1} + I_2e^{-t/\tau 2}$, where I_1 and I_2 are intensities at different times, τ_1 and τ_2 are their corresponding lifetimes. The average lifetime (τ) is calculated using the equation, $\tau = (I_1\tau_1+I_2\tau_2)/(I_1+I_2)$. The quantum yield measurements were performed in quartz sample holder with appropriate excitation wavelength (the band maximum of excitation spectra), and collected emission wavelength from 400 nm to 850 nm using an absolute quantum yield measurement system (Hamamatsu, Model C11347-11). A monochromatic light source was used as the excitation light source, which mounted a xenon lamp with a lamp rating of 150W. The overall quantum yield $\Phi_{overall}$ is given by

$$\Phi_{overall} = \frac{S(Em)}{S(Abs)} = \frac{\int \frac{\lambda}{hc}\left[I_{em}^{sample}(\lambda) - I_{em}^{reference}(\lambda)\right]d\lambda}{\int \frac{\lambda}{hc}\left[I_{ex}^{reference}(\lambda) - I_{ex}^{sample}(\lambda)\right]d\lambda} \quad (1)$$

where S(Abs) is the number of photons absorbed by a sample and S(Em) is the number of photons emitted from a sample, λ is the wavelength, h is Planck's constant, c is the velocity of light, $I_{sample\ (ex)}$ and $I_{reference\ (ex)}$ are the integrated intensities of the excitation light with and without a sample respectively, $I_{sample\ (em)}$ and $I_{reference\ (em)}$ are the photoluminescence intensities with and without a sample, respectively.

Synthesis of ligand

The ligand triCB-NTB (4,4',4''-(2,2',2''-nitrilotris(methylene)tris(1*H*-benzo[*d*]imidazole-2,1-diyl)tris(methylene))tribenzoic acid, denoted as H_3L herein) were synthesized according to our earlier report.[14]

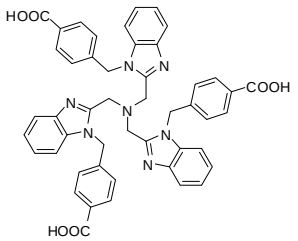

Scheme 1. Structure of the ligand triCB-NTB (**H_3L**).

Synthesis of complexes

Series I: Pb_2LnL_2 series

$[Pb_2TbL_2](NO_3)\cdot 2DMF\cdot 5H_2O$ (complex **Pb_2TbL_2**). A mixture of ligand **H_3L** (0.1 mmol), $Pb(NO_3)_2\cdot 6H_2O$ (0.1 mmol), $Tb(CF_3SO_3)_3\cdot 6H_2O$ (0.05 mmol) and DMF/H_2O (2 mL / 2 mL) was sealed in a 15 ml Teflon-lined stainless steel container. The container was heated to 120 °C and held at that temperature for 50 h, and then cooled to 30 °C at a rate of 5 °C h^{-1}. Colorless crystals of **Pb_2TbL_2** were collected in 40% yield. Anal. Calc. (%) for $[Pb_2Tb(C_{48}H_{36}N_7O_6)_2(NO_3)](C_3H_7NO)_2(H_2O)_5$: N 9.58; C 49.29; H 3.89. Found: N 9.68; C 49.86; H 3.98.

$[Pb_2EuL_2](NO_3)\cdot 2DMF\cdot 3H_2O$ (complex **Pb_2EuL_2**). Complex **Pb_2EuL_2** was obtained from the same procedure as that of **Pb_2TbL_2**, unless $Eu(CF_3SO_3)_3\cdot 6H_2O$ was used instead of $Tb(CF_3SO_3)_3\cdot 6H_2O$. Yield, 35%. Anal. Calc. (%) for $[Pb_2Eu(C_{48}H_{36}N_7O_6)_2(NO_3)](C_3H_7NO)_2(H_2O)_3$: N 9.75; C 50.16; H 3.80. Found: N 9.88; C 50.36; H 3.94.

$[Pb_2SmL_2](NO_3)\cdot 2DMF\cdot 2H_2O$ (complex **Pb_2SmL_2**). Complex **Pb_2SmL_2** was obtained from the same procedure as that of **Pb_2TbL_2**, unless $Sm(CF_3SO_3)_3\cdot 6H_2O$ was used instead of $Tb(CF_3SO_3)_3\cdot 6H_2O$. Yield, 38%. Anal. Calc. (%) for $[Pb_2Sm(C_{48}H_{36}N_7O_6)_2(NO_3)](C_3H_7NO)_2(H_2O)_2$: N 9.83; C 50.57; H 3.74. Found: N 9.88; C 50.26; H 3.80.

$[Pb_2GdL_2](NO_3)\cdot 2DMF\cdot 3H_2O$ (complex **Pb_2GdL_2**). Complex **Pb_2GdL_2** was obtained from the same procedure as that of **Pb_2TbL_2**, unless $Gd(CF_3SO_3)_3\cdot 6H_2O$ was used instead of $Tb(CF_3SO_3)_3\cdot 6H_2O$. Yield, 42%. Anal. Calc. (%) for $[Pb_2Gd(C_{48}H_{36}N_7O_6)_2(NO_3)](C_3H_7NO)_2(H_2O)_3$: N 9.73; C 50.05; H 3.79. Found: N 9.78; C 50.26; H 3.90.

Series II: $PbLn_2L_2$ series

$[PbTb_2L_2(NO_3)_2]\cdot 4DMF\cdot 6H_2O$ (complex **$PbTb_2L_2$**). A mixture of ligand **H_3L** (0.1 mmol), $Pb(NO_3)_2\cdot 6H_2O$ (0.05 mmol), $Tb(CF_3SO_3)_3\cdot 6H_2O$ (0.1 mmol) and DMF/H_2O (2 mL / 2 mL) was sealed in a 15 ml Teflon-lined stainless steel container. The container was heated to 120 °C and held at that temperature for 50 h, and then cooled to 30 °C at a rate of 5 °C h^{-1}. Colorless crystals of **$PbTb_2L_2$** were collected in 51% yield. Anal. Calc. (%) for $[PbTb_2(C_{48}H_{36}N_7O_6)_2(NO_3)_2](C_3H_7NO)_4(H_2O)_6$: N 10.52; C 48.71; H 4.24. Found: N 10.63; C 48.87; H 4.24.

$[PbEu_2L_2(NO_3)_2]\cdot 4DMF\cdot 8H_2O$ (complex **$PbEu_2L_2$**). Complex **$PbEu_2L_2$** was obtained from the same procedure as that of **$PbTb_2L_2$**, unless $Eu(CF_3SO_3)_3\cdot 6H_2O$ was used instead of $Tb(CF_3SO_3)_3\cdot 6H_2O$. Yield, 50%. Anal. Calc. (%) for $[PbEu_2(C_{48}H_{36}N_7O_6)_2(NO_3)_2](C_3H_7NO)_4(H_2O)_8$: N 10.43; C 48.31; H 4.35. Found: N 10.48; C 48.35; H 4.30.

$[PbSm_2L_2(NO_3)_2]\cdot 4DMF\cdot 4H_2O$ (complex **$PbSm_2L_2$**). Complex **$PbSm_2L_2$** was obtained from the same procedure as that of **$PbTb_2L_2$**, unless $Sm(CF_3SO_3)_3\cdot 6H_2O$ was used instead of $Tb(CF_3SO_3)_3\cdot 6H_2O$. Yield, 45%. Anal. Calc. (%) for $[PbSm_2(C_{48}H_{36}N_7O_6)_2(NO_3)_2](C_3H_7NO)_4(H_2O)_4$: N 10.73; C 49.70; H 4.17. Found: N 10.68; C 49.17; H 4.20.

$[PbGd_2L_2(NO_3)_2]\cdot 4DMF\cdot 6H_2O$ (complex **$PbGd_2L_2$**). Complex **$PbGd_2L_2$** was obtained from the same procedure as that of **$PbTb_2L_2$**, unless $Gd(CF_3SO_3)_3\cdot 6H_2O$ was used instead of $Tb(CF_3SO_3)_3\cdot 6H_2O$. Yield, 50%. Anal. Calc. (%) for $[PbGd_2(C_{48}H_{36}N_7O_6)_2(NO_3)_2](C_3H_7NO)_4(H_2O)_6$: N 10.53; C 48.77; H 4.24. Found: N 10.50; C 48.69; H 4.21.

Crystallography

Single-crystal reflection data were collected on an Agilent Gemini S Ultra diffractometer with the Enhanced X-ray Source of Cu-Kα radiation (λ = 1.54178 Å) using the ω-φ scan technique at 293 K. Empirical absorption correction was applied using spherical harmonics implemented in SCALE3 ABSPACK scaling algorithm. Structural solution and refinement against F^2 were carried out using the SHELXL programs.[17] All the non-hydrogen atoms were refined with anisotropic parameters, while H atoms were placed in calculated positions and refined using a riding model, except for the H atoms of water molecules, which were found by electron cloud density (Q peaks). Crystallographic data and structural refinement information are listed in Table 1. The selected bond lengths and bond angles for compounds are listed in Table S1. Crystallographic data for the structures reported in this paper have been deposited with the Cambridge Crystallographic Data Centre as supplementary publication no. 1043820-1043822.

Table 1. The crystal data and structure refinement summary for complexes.

Complex	Pb_2TbL_2	Pb_2EuL_2	$PbTb_2L_2$
Formula	$C_{102}H_{90}N_{16}O_{19}Pb_2Tb$	$C_{102}H_{90}EuN_{16}O_{19}Pb_2$	$C_{108}H_{100}N_{20}O_{28}PbTb_2$
Formula weight	2417.19	2410.23	2651.10
Crystal system	Monoclinic	Monoclinic	Triclinic

Space group	$P2_1/n$	$P2_1/n$	P-1
a (Å)	12.3263(1)	12.31597(16)	11.7061(5)
b (Å)	20.7018(2)	20.8623(2)	13.0527(4)
c (Å)	18.2517(2)	18.2267(2)	17.9550(8)
α (°)	90.00	90.00	87.730(3)
β(°)	91.642(1)	91.6890(11)	88.010(4)
γ(°)	90.00	90.00	89.886(3)
Volume ($Å^3$)	4655.49(8)	4681.11(10)	2739.65(19)
Z	2	2	1
Dcalc (g cm^{-3})	1.724	1.710	1.607
μ (mm^{-1})	11.259	12.278	9.890
Goodness-of-fit on F2	1.058	0.883	1.079
*R*1[*I*>2σ(*I*)]	0.0400	0.0361	0.0410
w*R*2(all data)	0.1139	0.1162	0.1119

Acknowledgements

This work was supported by the National Basic Research Program of China (973 Program, 2012CB821701), NSF of China (91222201, 21373276), the RFDP of Higher Education of China, and the Fundamental Research Funds for the Central Universities (15lgzd05).

Notes and references

[a] MOE Laboratory of Bioinorganic and Synthetic Chemistry, State Key Laboratory of Optoelectronic Materials and Technologies, School of Chemistry and Chemical Engineering, Sun Yat-Sen University, Guangzhou 510275, China, Email: panm@mail.sysu.edu.cn
[b] State Key Laboratory of Structural Chemistry, Fujian Institute of Research on the Structure of Matter, Chinese Academy of Sciences, Fuzhou, Fujian 350002, China

Electronic Supplementary Information (ESI) available: [PXRD, more crystal structure graphs, luminescence spectra of the ligand and crystallographic information]. See DOI: 10.1039/b000000x/

1 (*a*) S. F. Lim, R. Riehn, W. S. Ryu, N. Khanarian, C. K. Tung, D. Tank, R. H. Austin, *Nano Lett.*, 2006, **6**, 169; (*b*) P. Zhang, W. Steelant, M. Kumar, M. Scholfield, *J. Am. Chem. Soc.*, 2007, **129**, 4526; (*c*) H. B. Wu, L. Ying, W. Yang and Y. Cao, *Chem. Soc. Rev.*, 2009, **38**, 3391; (*d*) K. T. Kamtekar, A. P. Monkman and M. R. Bryce, *Adv. Mater.*, 2010, **22**, 572; (*e*) M. J. Bowers, J. R. McBride, S. J. Rosenthal, *J. Am. Chem. Soc.*, 2005, **127**, 15378; (*f*) J. Liu, Q. G. Zhou, Y. X. Cheng, Y. H. Geng, L. X. Wang, D. G. Ma, X. B. Jing, F. S. Wang, *Adv. Mater.*, 2005, **17**, 2974; (*g*) Z. Mao, D. Wang, Q. Lu, W. Yu and Z. Yuan, *Chem. Commun.*, 2009, 346.

2 (*a*) A. Ablet, S. M. Li, Wei Cao, X. J. Zheng, W. T. Wong, L. P. Jin, *Chem. Asian J.*, 2013, **8**, 95; (*b*) F. Zhao, N. Sun, H. Zhang, J. Chen, D. Ma, *J. Appl. Phys*., 2012, **112**, 084504.

3 (*a*) D. Zhao, S.-J. Seo, B.-S. Bae, *Adv. Mater*., 2007, **19**, 3473; (*b*) Y. J. Wada, M. Sato, Y. Tsukahara, *Angew. Chem. Int. Ed*., 2006, **45**, 1925; (*c*) L. D. Carlos, R. A. Sa Ferreira, J. P. Rainho, V. De Zea Bermudez, *Adv. Funct. Mater.*, 2002, **12**, 819.

4 (*a*) M. Roushan, X. Zhang and J. Li, *Angew. Chem., Int. Ed.*, 2012, **51**, 436; (*b*) X. Fang, M. Roushan, R. Zhang, J. Peng, H. Zeng, and J. Li, *Chem. Mater.*, 2012, **24**, 1710.

5 (*a*) Y. Wada, M. Sato and Y. Tsukahara, *Angew. Chem. Int. Ed.*, 2006, **45**, 1925; (*b*) Y. S. Zhao, H. Fu, F. Hu, A. Peng, W. Yang and J. Yao, *Adv. Mater.*, 2008, **20**, 79.

6 (*a*) P. Coppo, M. Duati, V. N. Kozhevnikov, J. W. Hofstraat and L. De Cola, *Angew. Chem. Int. Ed.*, 2005, **44**, 1806; (*b*) Y. Liu, M. Pan, Q.-Y. Yang, L. Fu, K. Li, S.-C. Wei and C.-Y. Su, *Chem. Mater.*, 2012, **24**, 1954; (*c*) Q.-Y. Yang, K. Wu, J.-J. Jiang, C.-W. Hsu, M. Pan, J.-M. Lehn and C.-Y.Su, *Chem. Commun.*, 2014, **50**, 7702.

7 (*a*) H. Zhang, X. Shan, L. Zhou, P. Lin, R. Li, E. Ma, X. Guo and S. Du, *J. Mater. Chem. C*, 2013, **1**, 888; (*b*) Z.-F. Liu, M.-F. Wu, S.-H. Wang, F.-K. Zheng, G.-E. Wang, J. Chen, Y. Xiao, A-Q. Wu, G.-C. Guo and J.-S. Huang, *J. Mater. Chem. C*, 2013, **1**, 4634; (*c*) S.-L. Zhong, R. Xu, L.-F. Zhang, W.-G. Qu, G.-Q. Gao, X.-L. Wu and A.-W. Xu, *J. Mater. Chem.*, 2011, **21**, 16574.

8 (*a*) S. Dang, J.-H. Zhang and Z.-M. Sun, *J. Mater. Chem*., 2012, **22**, 8868; (*b*) G. J. He, D. Guo, C. He, X. L. Zhang, X. W. Zhao and C. Y. Duan, *Angew. Chem., Int. Ed.*, 2009, **48**, 6132; (*c*) Y.-H. Zhang, X. Li and S. Song, *Chem. Commun.*, 2013, **49**, 10397.

9 D. F. Sava, L. E. S. Rohwer, M. A. Rodriguez and T. M. Nenoff, *J. Am. Chem. Soc.*, 2012, **134**, 3983.

10 Y. H. Zhao, H. B. Xu, Y.-M. Fu, K.-Z. Shao, S.-Y. Yang, Z.-M. Su, X.-R. Hao, D.-X. Zhu and E.-B. Wang, *Cryst. Growth Des.,* 2008, **8**, 3566.

11 V. Stavila, K. H. Whitmire, I. Rusakova, *Chem. Mater.*, 2009, **21**, 5456.

12 A. C. Wibowo, S. A. Vaughn, M. D. Smith and H.-C. zur Loye, *Inorg. Chem.*, 2010, **49**, 11001.

13 J. He, M. Zeller, A. D. Hunter and Z. Xu, *J. Am. Chem. Soc.*, 2012, **134**, 1553.

14 C. Yan, K. Li, S.-C. Wei, H.-P. Wang, L. Fu, M. Pan and C.-Y. Su, *J. Mater. Chem.*, 2012, **22**, 9846.

15 (*a*) N. S. Singh, R. S. Ningthoujam, G. Phaomei, S. D. Singh, A. Vinu and R. K. Vatsa, *Dalton Trans.*, 2012, **41**, 4404; (*b*) A. K. Parchur, A. I. Prasad, S. B. Rai and R. S. Ningthoujam, *Dalton Trans.*, 2012, **41**, 13810; (*c*) G. Phaomei, W. R. Singh, R. S. Ningthoujam, *J. Lumin.*, 2011, **131**, 1164.

16 (*a*) M. Pan, X.-L. Zheng, Y. Liu, W.-S. Liu and C.-Y. Su, *Dalton Trans.*, 2009, 2157; (*b*) D. P. Dutta, R. S. Ningthoujam, A. K. Tyagi, *AIP Adv.*, 2012, **2**, 042184; (*c*) L. P. Singh, S. K. Srivastava, R. Mishra, and R. S. Ningthoujam, *J. Phys. Chem. C*, 2014, **118**, 18087.

17 G. M. Sheldrick, SHELX-97, Program for refinement of crystal structures, University of Göttingen, Germany, 1997.